Green Synthesis of NiO/CuO Nanocomposites with a Snow Flake-Like Shape Morphology, Biological and Photocatalytic Activities Utilizing Vitex Negundo Leaf Extract

Hajeera Aseen A
Vels Institute of Science Technology and Advanced Studies
Sridevi D
Vels Institute of Science Technology and Advanced Studies
Jegadheeshwari S
SRM Institute of Science and Technology
Kesavan M
SRM Institute of Science and Technology
Jyolsna P
Vels Institute of Science Technology and Advanced Studies
Parthasarathy M
Vels Institute of Science Technology and Advanced Studies
Gowthami V
gowthamivijayakumar@gmail.com

Vels Institute of Science Technology and Advanced Studies

Research Article

Keywords: Green synthesis, NiO/CuO nanocomposites, Physical studies, Biological and Photo catalytic Applications

Posted Date: June 16th, 2025

DOI: https://doi.org/10.21203/rs.3.rs-6760909/v1

Additional Declarations: No competing interests reported.

Abstract

The sustainable synthesis of NiO/CuO nanocomposite was successfully achieved by utilising Vitex negundo leaf extract, presenting an environmentally friendly approach to pollution prevention. The nanocomposites were systematically prepared in varying compositions. X-ray diffraction (XRD) and Fourier-transform infrared (FTIR) spectroscopy analyses confirmed the crystalline structure and identified the functional groups present within the material. Additionally, ultraviolet-visible (UV-vis) spectroscopic analysis was conducted to determine the characteristic absorbance peaks and corresponding band gaps. Electron microscopy analysis demonstrated that the NiO/CuO nanocomposite displays a distinctive snowflake-like morphology. The antibacterial efficacy of the synthesised nanocomposite was assessed against Staphylococcus aureus, Escherichia coli, Klebsiella pneumoniae, and Enterobacter. Furthermore, a red blood cell (RBC) membrane stabilisation assay evaluated the potential anti-inflammatory effects. The photocatalytic efficiency of the nanocomposite was investigated using methylene blue (MB) dye under visible light irradiation. The green-synthesized material exhibited significant antibacterial, anti-inflammatory, and photocatalytic activities.

1 INTRODUCTION

Nanotechnology encompasses the science and engineering involved in creating and manipulating materials at the nanometer scale, which is one billionth of a meter. This field exploits the unique properties exhibited by materials at this scale to foster the development of advanced applications in medicine, electronics, materials science, and energy. In recent years, the synthesis of nanoparticles and nanocomposites has emerged as a critical area of research within materials science due to their distinct properties and wide-ranging applications. Nanocomposites, which are formed by embedding nanoparticles within a matrix, demonstrate enhanced biological and functional attributes owing to synergistic interactions, thereby rendering them suitable for various biological applications [1–5].

Green synthesis has gained substantial prominence among the various synthesis methodologies due to its environmentally friendly and sustainable nature. This approach utilises biological materials, including plant extracts, fruit peels, bacteria, fungi, and algae, to produce nanoparticles, thereby avoiding the toxic chemicals and harsh physical conditions commonly associated with traditional synthesis methods. The environmentally benign characteristics of green synthesis contribute to a reduced ecological footprint and enhanced biocompatibility of the resultant nanoparticles, making them appropriate for various biological uses. This method takes advantage of biological entities' natural reducing, capping, and stabilising agents. Notably, plant extracts are abundant in bioactive compounds such as flavonoids, alkaloids, terpenoids, and polyphenols, which effectively mediate the reduction of metal ions into their corresponding nanoparticles [6–9]. The green synthesis approach is both cost-effective and scalable, and it can produce nanoparticles with controlled size and morphology. Nickel oxide (NiO) nanoparticles are notable for their excellence across several domains, including optical, functional, and biological applications. Due to their inherent stability and reactivity, these nanoparticles exhibit potential antimicrobial activity, drug delivery capabilities, and biosensing applications [10–14]. Similarly, copper oxide (CuO) nanoparticles are renowned for their impressive antibacterial, antifungal, and antiviral properties. Their extensive surface area and high reactivity render them effective for catalysis, sensing, and environmental remediation. Furthermore, CuO nanoparticles are employed in various biomedical applications, such as cancer therapy and wound healing, attributable to their biocompatibility and therapeutic potential [15–19]. In this context, combining NiO and CuO nanoparticles into a nanocomposite synergistically enhances their individual properties, culminating in improved efficacy in biological applications. This synergistic effect arises from interactions between NiO and CuO at the nanoscale, which leads to enhanced charge transfer, stability, and reactivity [20–21]. The present study is centred on the green synthesis of NiO nanoparticles, which are incorporated with CuO nanoparticles utilising Vitex negundo (VN) leaf extract, commonly recognised as the Chinese chaste tree, widely acknowledged for its medicinal applications. The extract is particularly rich in phytochemicals such as flavonoids, glycosides, and essential oils, which confer various therapeutic properties, including anti-inflammatory, antioxidant, and antimicrobial activities. The employment of Vitex negundo leaf extract in the synthesis of nanoparticles harnesses these bioactive compounds for metal ion reduction and imparts additional medicinal properties to the synthesised nanoparticles [22–24].

In this investigation, the CuO/NiO nanocomposites were characterised using various techniques, including X-ray diffraction (XRD), Fourier transform infrared spectroscopy (FTIR), Ultraviolet-visible (UV-Vis) spectroscopy, and High-resolution scanning electron microscopy (HR-SEM) supplemented with Energy-dispersive X-ray (EDX) spectroscopic analysis. These methods were employed to ascertain the nanocomposites' structural, functional, optical, and morphological properties. The antibacterial, anti-inflammatory, and photocatalytic activities were evaluated using bacterial strains, RBC membrane stabilisation assays, and methylene blue degradation studies.

2 Characterization techniques

X-ray diffractometer (Panalytical, Netherlands) was studied using for an information on crystal structure and phase of NiO/CuO compositions over a 2 θ range of 10°– 80°. Fourier transform Infrared (FT-IR) spectra were recorded using an IR tracer 100 (Shimadzu) in the range of 4000 to 400 cm^{-1} (KBr pellet method). A Shimadzu UV 3600 plus spectrophotometer used to measuring the UV–vis absorption in the range is 200–800 nm. HR-SEM images were captured using a Thermo scientific Apreo S high-resolution scanning electron microscope at magnification 500 nm, 1μm, and 5μm.

2.1 X-ray diffraction analysis

X-ray diffraction (XRD) analysis was performed to analyse structural properties of the synthesized materials, and the spectrum are shown in the (Fig. 1). It reveals that NiO NPs distinct peaks are 37°, 43°, 62° and 75° corresponds to the crystal planes (111), (002), (202) and (113), indicates the face centered cubic in nature [25, 26]. CuO NPs distinct peaks are 35°, 38°, 48°, 53°, 58°, 61°, 66°, 68° and 72° corresponded to the crystal planes (002), (111), (-202), (020), (202), (-113), (-311), (113) and (311), indicates monoclinic in nature [27].

The prominent peak orientation along with (002) and (111) indicates that high crystallinity corresponding to CuO nanoparticles. The larger ionic radius of Cu^{2+} compared to Ni^{2+} might contribute to the strong crystallinity observed in CuO NPs. The observed patterns demonstrate how adjusting the molar ratio affects the phase composition. The A1 composition pattern displays a balanced combination of peaks from both NiO and CuO, indicating the successful formation of the nanocomposite with well-defined structures. The electrostatic interactions between charged species in the precursor solutions and the surface charges of the nanoparticles affect the nucleation and growth processes, ultimately influencing the crystalline structures observed in the XRD patterns. The balanced charge distribution in the 1:1 ratio (A1) may lead to a more uniform nucleation of both NiO and CuO phases [28]. A2 composition shows the intensity of the peaks decreases and the size of the nanoparticles increases with higher copper concentrations. This effect is due to the weakening of the internal structure, as the growth rate accelerates with increased concentration [25]. In A3 composition, the pattern shows dominant NiO peaks, reflecting a higher proportion of NiO relative to CuO. Higher concentration NiO peaks eliminate the CuO peaks (020), (-311), and (311).

The grain sizes of the particles in the NiO/CuO nanocomposites were estimated using the Scherrer equation:

$D = K \lambda / \beta \cos \theta$ (2)

Where λ is the wavelength of the radiation, K is a constant equal to 0.94, β is the peak width at half–maximum intensity and θ is the peak position. The average crystallite size of the NiO-CuO nanocomposite, calculated for different samples A1, A2, and A3, is denoted in Table 1, Table 2, and Table 3, correspondingly.

Table 1
Calculate the A1 sample average Scherrer value using XRD for NiO-CuO Nanocomposite

S.I no	2θ deg	hkl	θ deg	FWHM deg	D	Average D for NiO, nm	Average D for CuO, nm
1	35.291	002	17.6455	0.264	31.56543	26.26	26.69
2	36.867	111	18.4335	0.302	27.7175	(A1 sample)	
3	38.432	111	19.216	0.3	28.03249		
4	42.97	002	21.485	0.36	23.70613		
5	48.686	-202	24.343	0.322	27.06866		
6	58.279	202	29.1395	0.334	27.22124		
7	61.42	-113	30.71	0.342	27.00729		
8	62.7	202	31.35	0.369	25.19991		
9	66.29	-311	33.145	0.392	24.19492		
10	68.462	113	34.231	0.441	21.78007		
11	75.21	113	37.605	0.352	28.47662		

Table 2
Calculate the A2 sample average Scherrer value using XRD for NiO-CuO Nanocomposite

S.I no	2θ deg	hkl	θ deg	FWHM deg	D	Average D for NiO, nm	Average D for CuO, nm
1	35.206	002	17.603	0.302	27.58712	26.03	26.17
2	38.677	111	19.3385	0.365	23.05764	(A2 sample)	
3	48.686	-202	24.343	0.33	26.41245		
4	53.317	020	26.6585	0.295	30.1213		
5	58.02	202	29.01	0.351	25.8703		
6	62.01	202	31.005	0.341	27.16994		
7	66.29	-311	33.145	0.321	29.54644		
8	68.03	113	34.015	0.465	20.60323		
9	75.059	113	37.5295	0.402	24.90949		

Table 3
Calculate the A3 sample average Scherrer value using XRD for NiO-CuO Nanocomposite

S.I no	2θ deg	hkl	θ deg	FWHM deg	D	Average D for NiO, nm	Average D for CuO, nm
1	35.29	002	17.645	0.341	24.43768	26.40	25.36
2	36.92	111	18.46	0.311	26.91954	(A3 sample)	
3	38.51	111	19.255	0.338	24.88682		
4	42.97	002	21.485	0.339	25.17465		
5	48.77	-202	24.385	0.33	26.42122		
6	58.19	202	29.095	0.344	26.4185		
7	62.27	202	31.135	0.338	27.44859		
8	66.29	-311	33.145	0.321	29.54644		
9	68	113	34	0.467	20.51137		
10	75.14	113	37.57	0.384	26.0912		

2.2 FTIR analysis

Fourier Transform Infrared Spectroscopy (FTIR) is widely used analytical technique for identifying functional groups. The FTIR spectra of three different ratios of NiO nanoparticles composited with CuO nanoparticles represented in Fig. 2. In this Fig. 2 the wavenumbers 3430 cm^{-1} and 3434 cm^{-1} show broad peaks allocated to hydroxyl groups and O-H stretching vibrations of interlayer H_2O molecules. It plays a crucial role in materials science and chemistry and it improves the chemical reactivity and hydrophilicity of nanoparticles, making them appropriate for purposes in catalysis, drug delivery, and environmental remediation. The presence of these groups facilitates surface functionalization, allowing for the attachment of specific functional molecules or groups. The bands at 1646 cm^{-1} and 1636 cm^{-1} indicate the O-H bending vibrations of water molecules [29]. The intense bands observed at 2929 cm^{-1}, 2848 cm-1, 1383 cm^{-1}, 1384 cm^{-1}, and 1385 cm^{-1} probably due to the C–H stretching modes arising from the presence of surfactant molecules associated with the Cu Ni alloy nanoparticles [30]. A peak 1120 cm^{-1} confirms to stretching vibration of C-O [31]. The absorption peaks at 1033, 1086 cm^{-1} and 1090 cm^{-1} represent C-OH bending respectively [32]. The area from 1000 to 440 cm^{-1} demonstrates the stretching frequencies of metal-oxygen bonds. The peaks at 583 cm^{-1}, 585 cm^{-1}, 589 cm^{-1}, and 654 cm^{-1} indicate the presence of Ni-O and Cu-O metal-oxygen frequencies in the spectrum [33].

2.3 Optical analysis

The UV–Vis spectrum of NiO/CuO nanocomposites via green synthesis applying Vitex negundo (VN) leaf extract is exposed in Fig. 3. Pure NiO absorbs in the UV region (310–380 nm) due to its wide bandgap

(3.3–4.0 eV), while CuO absorbs in the visible-NIR region (590–1030 nm) with d–d transitions around 600–800 nm [34]. However, NiO/CuO nanocomposite shows absorption at 200–250 nm, likely due to phytochemical interactions from Vitex negundo extract, quantum confinement effects, heterojunction formation, and oxygen vacancies, which modify electronic transitions and enhance UV absorption. The VN extract contributes bioactive compounds, such as polyphenolics and flavonoids, with hydroxyl groups (O–H) that are known to absorb UV light [25, 35]. The Optical absorptions detected in the UV region (243 nm for A1, and 232 nm for A2 and A3) are attributed to the bandgap absorption of the nanoparticles. These observations align with the quantum confinement effect, where the particle size significantly influences the optical properties. The distinct interbond electronic transitions, primarily between $Ni^{2+}–O^{2-}$ and $Cu^{2+}–O^{2-}$, correspond to the material's wide bandgap semiconductor behaviour [34]. The Tauc's plots (Fig. 4) were used to calculate the optical bandgap values of the synthesized nanoparticles based on the indirect allowed transition, as both NiO and CuO exhibit indirect bandgap behaviour in bulk and nanoscale forms. The Tauc relation is given as:

$\alpha h\nu = A(h\nu - Eg)^n$ (3)

Where α is the absorption coefficient, $h\nu$ is the photon energy, A is a proportionality constant, Eg is the optical bandgap, and n is the order of transitions.

The calculated bandgaps values for A1, A2, and A3 are 5.56 eV, 5.01 eV, and 5.25 eV respectively. These variations are influenced by quantum confinement, where smaller particles result in higher energy gap. The NiO/CuO composition plays a key role, copper incorporation introduces structural defects, affecting oxygen vacancies and charge trapping states, thereby lowering the bandgap. A higher CuO concentration correlates with a decreased bandgap [28].

UV-Vis absorption analysis reveals a blueshift in A2 and A3 due to the Burstein- Moss effect, confirming quantum confinement while the red shift in A1 suggests larger particle size is confirmed by Scherrer formula [36].

2.4 HR-SEM and EADX analysis

The green synthesis of NiO nanoparticles nano composed with CuO nanoparticles using Vitex Negundo leaf extract was performed with different composites (A1, A2, and A3) and different magnifications (500 nm, 1 μm, and 3 μm) as shown in Figs. 1, 2 and 3. In the A1 composites SEM characterization of the NiO-CuO nanocomposite with an equal ratio, the heterogeneous structure reflects the interplay between NiO isotropic growth, leading to nanorod shape, and CuO anisotropic growth, forming hexagonal structure shown in in Fig. 5. This variation in morphology highlights the distinct crystallization behaviours of the two materials, resulting in a composite with diverse structural features that could enhance its functional properties [37, 38].

The SEM images of the A2 sample show that the snowflake-like structure observed in the NiO-CuO nanocomposite arises due to the dominant crystallization behavior of CuO, which is present in higher concentrations. CuO tends to nucleate and grow more extensively, developing complex hierarchical structures due to its anisotropic crystal growth in the monoclinic phase. The lower concentration of NiO, which is typically nanorod in shape, subtly influences this process, acting as a secondary nucleation site and changing the growth pattern of CuO are shown in Fig. 6. The differences in surface energy between NiO and CuO also contribute to the unique morphology, with CuO higher surface energy promoting more prominent crystal growth. Snowflake structure likely represents a balance between thermodynamic stability and kinetic control during synthesis. Vitex negundo leaf extract, rich in polyphenols, flavonoids, and other bioactive compounds, plays a vital role in this synthesis. These poly chemicals not only act as reducing and capping agents but also impact the crystallization dynamics, contributing to the formation of the unique snowflake-like morphology. This eco-friendly synthesis approach enhances the efficient properties of the nanocomposite, making it suitable for applications in biomedical fields such as antibacterial and antioxidant therapies, as well as in photocatalytic degradation of environmental pollutants [39, 40].

A3 composites the SEM images illustrate that as the concentration of NiO increases, the particles exhibit a slightly spherical, and CuO concentration shows the particles are hexagonal in shape. At different magnifications, the particles appear small, and evenly distributed, with agglomeration are given in Fig. 7. The CuO content is reduced as the NiO content is increased thereby representing the presence of an increasing amount of NiO [41].

The EDAX spectrum analysis indicates that the sample predominantly consists of nickel oxide (NiO) nanoparticles, with an atomic ratio of 32 at% nickel (Ni) and 42 at% oxygen (O), suggesting a higher nucleation density of NiO within the composite matrix. The remaining 26 at% of the atomic composition corresponds to copper oxide (CuO) nanoparticles, which may influence the overall structural and catalytic properties of the material. Notably, no impurity peaks were observed, confirming the purity of the synthesized composite.

The EDAX analysis of the NiO/CuO nanocomposite reveals that the material is primarily composed of oxygen (54.11 at%), copper (40.44 at%), and nickel (5.44 at%), with no significant impurities detected. The high copper content, indicated by both the weight and atomic percentages, suggests that CuO is the dominant phase in the composite, while the presence of oxygen and nickel confirms the successful formation of the NiO phase. The elemental ratio of Ni to Cu, based on atomic percentages reflects the higher proportion of copper in the nanocomposite. These results verify the intended stoichiometry of the synthesized NiO/CuO nanocomposite, supporting its potential applications in areas such as antibacterial activity. The EDAX analysis of the NiO/CuO nanocomposite indicates that the sample is primarily composed of copper (38.71 at%), oxygen (48.94 at%), and nickel (12.35 at%). The presence of oxygen and nickel, at appropriate ratios, confirms the successful formation of NiO alongside CuO. The Cu atomic percentage increased; the Ni atomic percentages decreased because of the ionic radii which is observed in XRD analysis [41].

2.5 Biological activities

2.5.1. Antibacterial activity

Table 4
Antibacterial activity of NiO/CuO nanocomposites (mm inhibition zones)

Gram - positive	BACTERIAS	DMSO	CONTROL	NiO-CuO A1	NiO-CuO A2	NiO-CuO A3
	Staphylococcus aureus	00	13	10	15	11
Gram - negative	**Escherichia coli**	00	12	13	13	11
	Klebsiella pneumoniae	00	15	11	18	12
	Enterobacter	00	12	10	12	12

The synthesized NiO/CuO NPs were tested for their antibacterial activity against harmful Gram-negative strains (E. coli, K. pneumonia, and Enterobacter) and Gram-positive strains (S. aureus) [42]. After 24 hours of inoculation, the modification in antibacterial effectiveness between the three ratios. In Fig. 9 + ve control represents the chloramphenicol. The A2 nanocomposite showed the highest antibacterial activity, with inhibition regions of 15 mm against Staphylococcus aureus and 18 mm alongside Klebsiella pneumoniae. This significantly outperformed both A1 and A3 as well as the positive control. A1 exhibited mediate activity with inhibition zones of 13 mm for both Escherichia coli and K. pneumoniae, while A3 showed lower activity, with 11 mm zones against S. aureus and E. coli, and 12 mm against K. pneumoniae. The improved functioning of the A2 nanocomposite is recognized for its enhanced composition, which facilitates higher reactive oxygen species generation, leading to oxidative stress and bacterial membrane disruption. The Vitex negundo leaf extract, rich in polyphenols and flavonoids, plays a critical role in this synthesis by acting as a natural reducing and capping agent, manipulating illustration dynamics and supporting the formation of the snowflake-like structure unique to A2 [43]. This structure provides a larger surface area and more active sites, enhancing antibacterial efficacy. Bacterial susceptibility plays a role, with Gram-negative bacteria (E. coli and K. pneumoniae) being more vulnerable to ROS-induced damage compared to Gram-positive S. aureus, which has a broader protective peptidoglycan layer [44].

2.5.2 Anti-inflammatory activity

The anti-inflammatory activity of NiO/CuO nanocomposite, synthesized via a green route utilizing Vitex negundo leaf extract, was evaluated through the different ratios compositions, a red blood cell (RBC) membrane stabilization assay [45]. Various molar ratios (A1, A2 and A3) of NiO to CuO were tested at concentrations from 100 to 500 µg/mL, with diclofenac sodium serving as the pharmacological standard [46]. The A2 sample, NiO/CuO nanocomposite demonstrated the highest hemolysis inhibition, reaching 55.2% at 500 µg/mL, closely paralleling diclofenac's benchmark inhibition of 70.3% under equivalent conditions. This pronounced anti-inflammatory effect is attributed to the rare physicochemical synergy between NiO and CuO, potentially augmenting bioactivity through enhanced stability and interaction at the cellular membrane. The phytochemicals in Vitex negundo likely contribute to the membrane-protective capacity of these nanocomposites, reinforcing their resistance against hypotonic-induced

RBC lysis. The sample A2 NiO/CuO composition as a bioactive nanocomposite for anti-inflammatory applications, affording a sustainable and biocompatible alternative to conventional therapeutic agents within the field of nanomedicine.

Table 5
Anti-inflammatory activity of NiO/CuO nanocomposites using vitex negundo leaf extract

Sample Concentration (μg)	100	200	300	400	500	B
Diclofenac	0.36	0.27	0.21	0.17	0.12	0.41
% of inhibition	12.1	34.1	48.7	58.5	70.3	
A1	0.35	0.33	0.31	0.29	0.27	
% of inhibition	7.8	13.1	18.4	23.6	28.9	
A2	0.32	0.28	0.25	0.21	0.17	
% of inhibition	15.7	26.3	34.2	44.7	55.2	
A3	0.33	0.30	0.28	0.25	0.21	
% of inhibition	13.1	21	26.3	34.2	44.7	

2.5.3 Photocatalytic activity

The photocatalytic degradation NiO/CuO nanocomposites was studied under solar irradiation to evaluate the of methylene blue (MB) dye [47]. A precise amount (1 mg) of methylene blue dye was dissolved in 100 mL of double-distilled water, and 25 mg of nanocomposite samples (ratios A1, A2 and A3) were added to 25 mL of the dye solution. A control experiment without the catalyst was maintained to follow natural degradation. The photocatalytic reactions were performed under direct sunlight, and aliquots were collected at time intervals of 0, 30, 60, 90, 120, and 150 minutes. UV-Vis spectrophotometric analysis at 660 nm was used to monitor the degradation of MB by quantifying the decrease in optical density (O.D). The concentration of MB was calculated using the Beer-Lambert law (A = εbc), where A is absorbance, ε is the molar extinction coefficient of MB, b is the path length, and c is the concentration.

The percentage of degradation (%D) was calculated using the equation [48],

$$\%\mathrm{D} = \left(\frac{\mathrm{C_0} - \mathrm{C_t}}{\mathrm{C_0}}\right) \times\ 100$$

4

where C_0 is the initial concentration of MB, and C_t is the concentration at time t.

The A2 sample, NiO/CuO nanocomposite exhibited the highest photocatalytic performance, achieving 66.67% degradation at 150 minutes, with a corresponding decrease in absorbance to 0.54, while the A1 and A3 sample showed 20% and 10% degradation, respectively. The enhanced activity of the A2 ratio is attributed to improved electron-hole pair separation due to the synergistic effect of NiO and CuO, which minimizes recombination losses and increases the generation of hydroxyl radicals (OH). These radicals are responsible for the degradation of MB through a series of redox reactions, where CuO acts as an electron acceptor and NiO facilitates electron transfer. Additionally, the degradation kinetics followed pseudo-first-order kinetics, with the reaction rate constant k calculated using the equation [49–51],

$$ln\left(\frac{c_0}{c_t}\right) = kt$$

5

This study demonstrated that the NiO/CuO nanocomposites, particularly the A2 sample, are highly effective for the photocatalytic degradation of organic dyes, making them promising materials for applications in wastewater treatment and environmental clean-up.

Table 6
Methylene Blue dye degradation

Sl.no	Time (min)	Methylene blue (O.D 660nm)			
		Control	1:1	1:3	3:1
1	0	1.15	1.20	1.20	1.22
2	30	1.10	1.07	1.03	1.06
3	60	1.05	1.04	0.95	1.00
4	90	1.00	1.00	0.88	0.95
5	120	1.00	0.98	0.69	0.92
6	150	1.00	0.95	0.44	0.90

Table 7
Comparison table for photocatalytic activity

S.I. no	nanoparticle	Synthesis method	dye	Time min	Degradation (%)	reference
1	NiO NPs	Co-precipitation	Methylene blue	300	60%	50
2	CuO NPs	Co-precipitation	Methyl orange	120	39%	51
3	NiO/CuO NPs	Green synthesis	Methylene blue	150	63%	Present study

3 Conclusion

NiO/CuO nanocomposites with three different compositions namely, (A1, A2, and A3) were synthesized using *Vitex negundo* leaf extract, developing agglomerates of snowflake-like particles. Characterization inveterate the nano compositing of NiO with a face-centered cubic structure and CuO with a monoclinic structure. Among the ratios, the A2 NiO/CuO nanocomposite demonstrated prominent antibacterial activity against *E. coli* and *K. pneumoniae* and reasonable anti-inflammatory activity in stabilizing human red blood cells, both of which were concentration-dependent. Additionally, A2 demonstrated outstanding photocatalytic efficiency in degrading methylene blue dye, highlighting its ability for ecological remediation. These properties suggest that NiO/CuO nanocomposites, particularly A2, could be explored for forthcoming purposes in biomedical fields, wastewater treatment, and catalytic processes.

Declarations

Acknowledgements: The authors thank all the experts of the Vels Institute of Science Technology and Advanced Studies, Chennai for their resilience in this research.

Author contributions:

A Hajeera Aseen: Conceptualisation, Methodology, Writing original draft;

D Sridevi: Data curation, Methodology;

S Jegadheeshwari: Methodology, Data curation;

M Kesavan: Methodology, Data curation;

P **Jyolsna**: Methodology, Data curation and formal analysis;

M Parthasarathy Methodology, and formal analysis;

V Gowthami: Overall Supervision, Investigation and Validation.

All authors reviewed the manuscript and accepted for publication.

Ethical approval

All experiments were carried out according to university guidelines. None of the authors used human beings as research subjects.

Consent for publication

In the present study, there were no person's data in any form.

Data availability

The data presented in this study are available upon request from the corresponding author.

Conflict of interest

The authors declare that they have no known competing financial interest or personal relationship that could have appeared to influence the work reported in this paper.

Funding Declaration Statement

The authors did not receive support from any organisation for the submitted work.

References

1. Chemingui H, Missaoui T, Mzali JC, Yildiz T, Konyar M, Smiri M, Yatmaz HC (2021) Green synthesis of metallic nanoparticles and their prospective biotechnological applications: an overview. Biol Trace Elem Res 199: 344-370. https://doi.org/10.1007/s12011-020-02138-3
2. Gour A, Jain NK (2019) Advances in green synthesis of nanoparticles. Artif Cells. Nanomed Biotechnol 47: 844-85. https://doi.org/10.1080/21691401.2019.1577878
3. Aldeen TS, Mohamed HEA, Maaza M (2022) ZnO nanoparticles prepared via a green synthesis approach: Physical properties, photocatalytic and antibacterial activity. J Phys Chem Solids 160: 110313. https://doi.org/10.1016/j.jpcs.2021.110313
4. Karam ST, Abdulrahman AF (2022) Green Synthesis and Characterization of ZnO Nanoparticles by Using Thyme Plant Leaf Extract. Photonics 9: 594. https://doi.org/10.3390/photonics9080594
5. Hussain I, Singh NB, Singh A, Singh H, Singh SC (2016) Green synthesis of nanoparticles and its potential application. Biotechnol Lett 38: 545-560. https://doi.org/10.1007/s10529-015-2026-7
6. Prakash M, Kavitha HP, Arulmurugan S, Vennila JP, Abinaya S, Lohita D, Rajendran AJCPI (2024) Green synthesis of gadolinium-doped bismuth oxide nanoparticles: Exploring their biological and photocatalytic activities. Chem Phys Impact 9:100678 https://doi.org/10.1016/j.cpi.2024.100678
7. Jyolsna P, Gowthami V (2024) Adsorption performance with field emission scanning electron microscopy of fruit peel induced Silver Nanoparticles in C16H18ClN3S for waste water treatment. MethodsX 13: 102951. https://doi.org/10.1016/j.mex.2024.102951
8. Samuel MS, Ravikumar M, John JA, Selvarajan E, Patel H, Chander PS, Chandrasekar NA (2022) review on green synthesis of nanoparticles and their diverse biomedical and environmental applications. Catalysts 12: 459. https://doi.org/10.3390/catal12050459
9. Ilbeigi G, Kariminik A, Moshafi MH (2019) The antibacterial activities of NiO nanoparticles against some gram-positive and gram-negative bacterial strains. Int j basic sci med 4: 69-74. https://doi.org/10.15171/ijbsm.2019.14
10. Nasseri MA, Ahrari F, Zakerinasab B (2016) A green biosynthesis of NiO nanoparticles using aqueous extract of Tamarix serotina and their characterization and application. Appl Organomet Chem 30: 978-984. https://doi.org/10.1002/aoc.3530

11. Siveswari A, Gowthami V (2024) Hierarchical NiCo2O4 needle-like heterostructure arrays anchored on WO3 as high-performance asymmetric supercapacitors for energy storage applications. Chem Phys Impact 9: 100666. https://doi.org/10.1016/j.chphi.2024.100666
12. Hong SJ, Mun HJ, Kim BJ, Kim YS (2021) Characterization of nickel oxide nanoparticles synthesized under low temperature. Micromachines 12: 1168. https://doi.org/10.3390/mi12101168
13. Iqbal J, Abbasi BA, Ahmad R, Mahmoodi M, Munir A, Zahra SA, Capasso R (2020) Phytogenic synthesis of nickel oxide nanoparticles (NiO) using fresh leaves extract of Rhamnus triquetra (wall.) and investigation of its multiple in vitro biological potentials. Biomed 8: 117. https://doi.org/10.3390/biomedicines8050117
14. Kumar PV, Shameem U, Kollu P, Kalyani RL, Pammi SVM (2015) Green synthesis of copper oxide nanoparticles using Aloe vera leaf extract and its antibacterial activity against fish bacterial pathogens. J Bionanosci 5: 135-139. https://doi.org/10.1007/s12668-015-0171-z
15. Ijaz F, Shahid S, Khan SA, Ahmad W, Zaman S (2017) Green synthesis of copper oxide nanoparticles using Abutilon indicum leaf extract: Antimicrobial, antioxidant and photocatalytic dye degradation activities. Trop J Pharm Res 16: 743-753. https://doi.org/10.4314/tjpr.v16i4.2
16. Rajendran A, Siva E, Dhanraj C, Senthilkumar SA (2018) green and facile approach for the synthesis copper oxide nanoparticles using Hibiscus rosa-sinensis flower extracts and it's antibacterial activities. J Bioprocess Biotech 8: 324. https://doi.org/10.4172/2155-9821.1000324
17. Vishveshvar K, Aravind Krishnan MV, Haribabu K, Vishnuprasad S (2018) Green synthesis of copper oxide nanoparticles using Ixiro coccinea plant leaves and its characterization. J Bionanosci 8: 554-558. https://doi.org/10.1007/s12668-018-0508-5
18. Vidovix TB, Quesada HB, Januário EFD, Bergamasco R, Vieira AMS (2019) Green synthesis of copper oxide nanoparticles using Punica granatum leaf extract applied to the removal of methylene blue. Mater Lett 257: 126685. https://doi.org/10.1016/j.matlet.2019.126685
19. Shanwaz MM, Shyam P (2022) Synthesis of silver nanoparticles from Vitex negundo plant by green method and their bactericidal effects. Lett Appl NanoBiosci 12: 59-62 https://doi.org/10.33263/LIANBS122.059
20. El-Shobaky GA, Radwan NR, El-Shall MS, Turky AM, Hassan HM (2007) The role of method of preparation of CuO–NiO system on its physicochemical surface and catalytic properties. Colloids Surf A Physicochem Eng Asp 311: 161-169. https://doi.org/10.1016/j.colsurfa.2007.04.014
21. Rahdar A, Aliahmad M, Azizi Y, Keikha N, Moudi M, Keshavarzi F (2017) CuO-NiO nano composites: synthesis, characterization, and cytotoxicity evaluation. Nanomed Res J 2: 78-86. https://doi.org/10.22034/nmrj.2017.56956.1057
22. Gill BS, Mehra R, Navgeet, Kumar S (2018) Vitex negundo and its medicinal value. Mol Biol Rep 4: 2925-293. https://doi.org/10.1007/s11033-018-4421-3
23. Khan MF, Arora P, Dhobi M (2021) A prospective review on phyto-pharmacological aspects of Vitex negundo Linn. Curr Tradit Med 7: 138-150. https://doi.org/10.2174/2215083805666191021161005

24. Gandhi PR, Jayaseelan C, Vimalkumar E, Mary RR (2016) Larvicidal and pediculicidal activity of synthesized TiO2 nanoparticles using Vitex negundo leaf extract against blood feeding parasites. J Asia Pac Entomol 19: 1089-1094. https://doi.org/10.1016/j.aspen.2016.10.001
25. S Ghazal (2021) Green synthesis of copper-doped nickel oxide nanoparticles using okra plant extract for the evaluation of their cytotoxicity and photocatalytic properties. Ceram Int 47: 27165-27176. https://doi.org/10.1016/j.ceramint.2021.06.135
26. Ponnusamy PM, Agilan S, Muthukumarasamy N, Senthil TS, Rajesh G, Venkatraman MR, Velauthapillai D (2016) Structural, optical and magnetic properties of undoped NiO and Fe-doped NiO nanoparticles synthesized by wet-chemical process. Mater. Charact 114: 166-171. https://doi.org/10.1016/j.matchar.2016.02.020
27. Arun L (2020) Optical, magnetic, electrical, and chemo-catalytic properties of bio-synthesized CuO/NiO nanocomposites. J Phys Chem Solids 136: 109155. https://doi.org/10.1016/j.jpcs.2019.109155
28. Varunkumar K (2017) Effect of calcination temperature on Cu doped NiO nanoparticles prepared via wet-chemical method: structural, optical and morphological studies. Mater Sci Semicond Process 66: 149-156. https://doi.org/10.1016/j.mssp.2017.03.014
29. El-Kemary M, Nagy N, El-Mehasseb I (2013) Nickel oxide nanoparticles: synthesis and spectral studies of interactions with glucose, Mater Sci Semicond Process 16: 1747-1752. https://doi.org/10.1016/j.mssp.2013.05.018
30. Ramya S, Viruthagiri G, Gobi R (2016) Synthesis and characterization of Ni^{2+} ions incorporated CuO nanoparticles and its application in antibacterial activity. J Mater Sci Mater Electron 27: 2701–2711. https://doi.org/10.1007/s10854-015-4080-2
31. Hussain T, Faisal S, Rizwan M, Zaman N, Iqbal M, Iqbal A, Ali Z (2022) Green synthesis and characterization of copper and nickel hybrid nanomaterials: Investigation of their biological and photocatalytic potential for the removal of organic crystal violet dye. J Saudi Chem Soc 26: 101486. https://doi.org/10.1016/j.jscs.2022.101486
32. Mohamed EA (2020) Green synthesis of copper & copper oxide nanoparticles using the extract of seedless dates. Heliyon 6: e03123.https://doi.org/10.1016/j.heliyon.2019.e03123
33. Yan B, Wang Y, Jiang T, Wu X (2016) Fabrication of snowflake-like CuO nanostructure via electrodeposition method and its properties, J Mater Sci Mater Electron 27: 4035-4042. https://doi.org/10.1007/s10854-015-4258-7
34. Weldekirstos HD, Habtewold B, Kabtamu DM (2022) Surfactant-assisted synthesis of NiO-ZnO and NiO-CuO nanocomposites for enhanced photocatalytic degradation of methylene blue under UV light irradiation. Front Mater Sci 9: 832439. https://doi.org/10.3389/fmats.2022.832439
35. Akbar I, Mullaivendhan J, Ahamed A, Aljawdah HM (2024) Vitex Negundo–Fe3O4–CuO green nanocatalyst (VN–Fe3O4–CuO): synthesis of pyrazolo [3, 4-c] pyrazole derivatives via the cyclization of isoniazid with pyrazole and their antimicrobial activity, cytotoxicity, and molecular docking studies, RSC Adv14: 677–688. https://doi.org/10.1039/D3RA06771H.

36. Singh M, Goyal M, Devlal K (2018) Size and shape effects on the band gap of semiconductor compound nanomaterials. J Taibah UnivSci 12: 470-475. https://doi.org/10.1080/16583655.2018.1473946
37. Nagajyothi PC, Muthuraman P, Sreekanth TVM, Kim DH, Shim J (2017) Green synthesis: in-vitro anticancer activity of copper oxide nanoparticles against human cervical carcinoma cells. Arab J Chem 10: 215-225. https://doi.org/10.1016/j.arabjc.2016.01.011
38. Faisal S (2021) Curcuma longa mediated synthesis of copper oxide, nickel oxide and Cu-Ni bimetallic hybrid nanoparticles: characterization and evaluation for antimicrobial, anti-parasitic and cytotoxic potentials. Coatings 11: 849. https://doi.org/10.3390/coatings11070849
39. Li X (2020) Diethylenetriamine-functionalized CdS nanoparticles decorated on Cu2S snowflake microparticles for photocatalytic hydrogen production. ACS Appl Nano Mater 3: 11517-11526. https://doi.org/10.1021/acsanm.0c02616
40. Parab H (2011) An anisotropic snowflake-like structural assembly of polymer-capped gold nanoparticles. J Nanoparticle Res 13: 2173-2180. https://doi.org/10.1007/s11051-010-9975-5
41. Arulkumar E, Shree SS, Thanikaikarasan S (2023) Structure, morphology, composition, optical properties of CuO/NiO nanocomposite for electrochemical energy storage devices. Results Chem 6: 101087.
42. Cacaci M, Biagiotti G, Toniolo G, Albino M, Sangregorio C, Severi M, Richichi B (2023) Shaping silver nanoparticles' size through the carrier composition: synthesis and antimicrobial activity. Nanomaterials 13: 1585. https://doi.org/10.3390/nano13101585
43. Yan J, Wang Q, Yang J, Rutter P, Xing M, Li B (2023) Chemical Synthesis of Innovative Silver Nanohybrids with Synergistically Improved Antimicrobial Properties. Int J Nanomedicine 2295-2305. https://doi.org/10.2147/IJN.S396019
44. Turlybekuly A, Pogrebnjak AD, Sukhodub LF, Sukhodub LB, Kistaubayeva AS, Savitskaya IS, Digel I (2019) Synthesis, characterization, in vitro biocompatibility and antibacterial properties study of nanocomposite materials based on hydroxyapatite-biphasic ZnO micro-and nanoparticles embedded in Alginate matrix Mater Sci Eng C 104: 109965. https://doi.org/10.1016/j.msec.2019.109965
45. Soliman TN, El-Dein AN, Abd Al-Diam S, Allayeh A, H. Awad, N.S. Flefil (2024) Characterization of C-phycocyanin antioxidant, anti-inflammatory, anti-tumour, and anti-HCoV-229E activities and encapsulation for implementation in an innovative functional yogurt. Heliyon 10: 31642. https://doi.org/10.1016/j.heliyon.2024.e31642
46. Adeyemi JO (2023) Kei-apple-mediated NiO nanoparticles and biological studies: anti-inflammatory and cytotoxicity study against HeLa and HEK 293 cell lines. Mater Res Express 10: 075401. https://doi.org/10.1088/2053-1591/acb8b1
47. Omotunde OI, Okoronkwo AE, Aiyesanmi AF, Gurgur E (2018) Photocatalytic behaviour of mixed oxide NiO/PdO nanoparticles toward degradation of methyl red in water. J Photochem Photobiol A 365: 145-150. https://doi.org/10.1016/j.jphotochem.2018.08.005

48. Ansari PMY (2023) Green synthesis of copper oxide nanoparticles using Amaranthus dubius leaf extract for sensor and photocatalytic applications. Chem Phys Impact 7: 100374. https://doi.org/10.1016/j.cphi.2023.100374
49. Bhuvaneshwari V (2024) Harnessing the potency of eco-friendly calcium oxide derived from eggshells for enhanced photocatalytic activity and biocompatibility evaluation in HepG2 cell line. Chem Phys Impact 9: 100699. https://doi.org/10.1016/j.chphi.2024.100699
50. Sabouri Z, Akbari A, Hosseini HA, Khatami M, Darroudi M (2020) Tragacanth-mediate synthesis of NiO nanosheets for cytotoxicity and photocatalytic degradation of organic dyes. Bioprocess Biosyst Eng 43:1209-1218. https://doi.org/10.1007/s00449-020-02315-7
51. Zeid EA, Ibrahem IA, Mohamed WA, Ali AM (2020) Study the influence of silver and cobalt on the photocatalytic activity of copper oxide nanoparticles for the degradation of methyl orange and real wastewater dyes. Mater Res Express7: 026201. https://doi.org/10.1088/2053-1591/ab7400

Figures

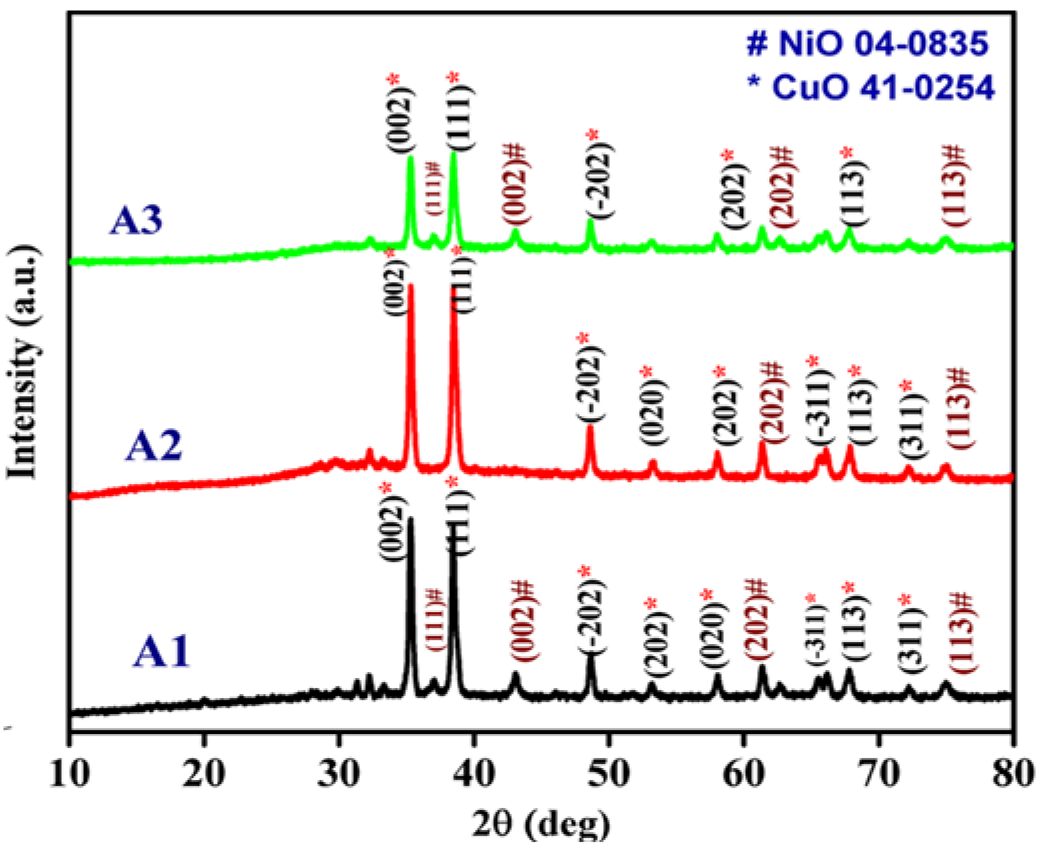

Figure 1

XRD pattern of NiO/CuO nanocomposites

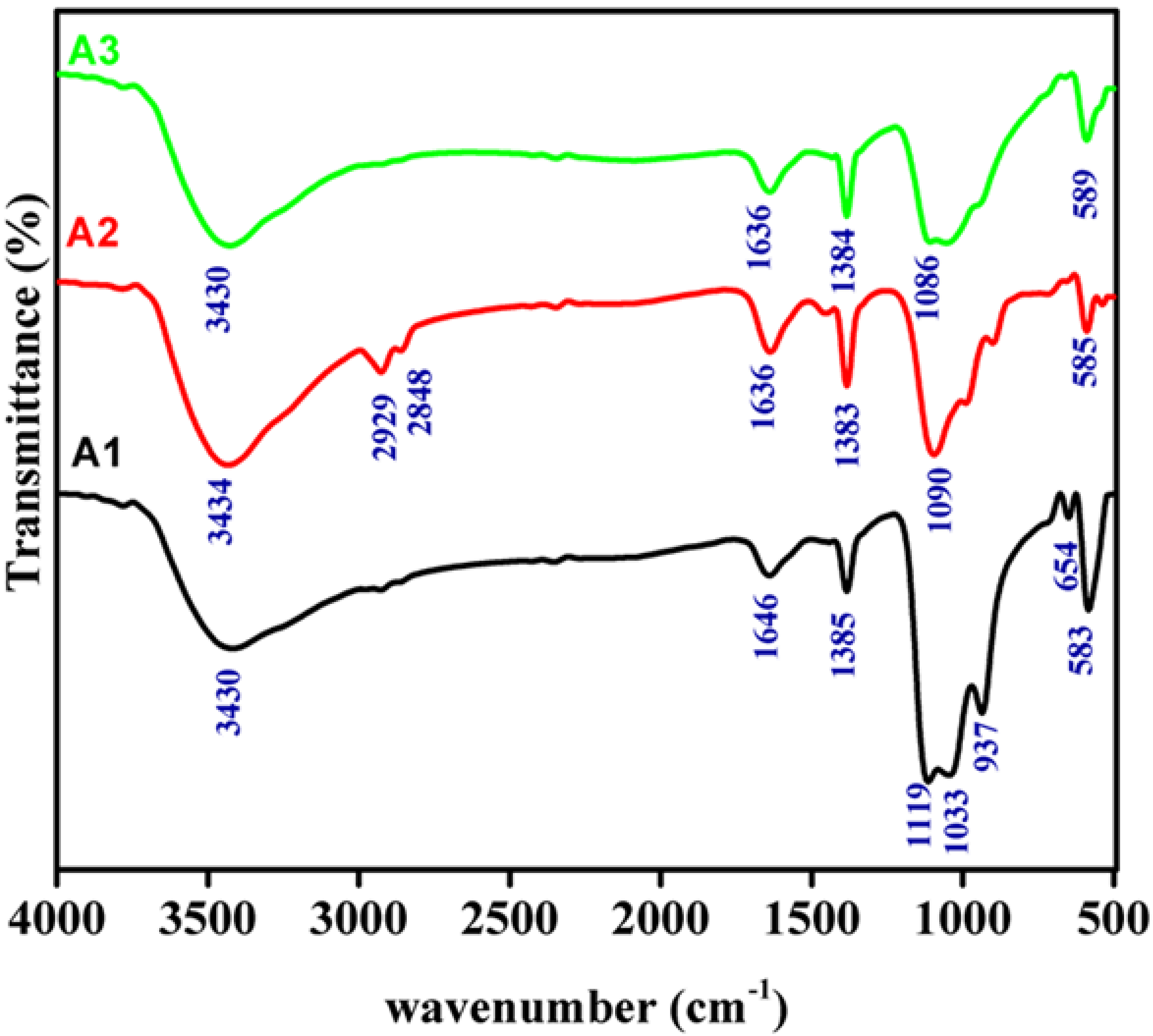

Figure 2

FTIR spectrum of prepared with different compositions

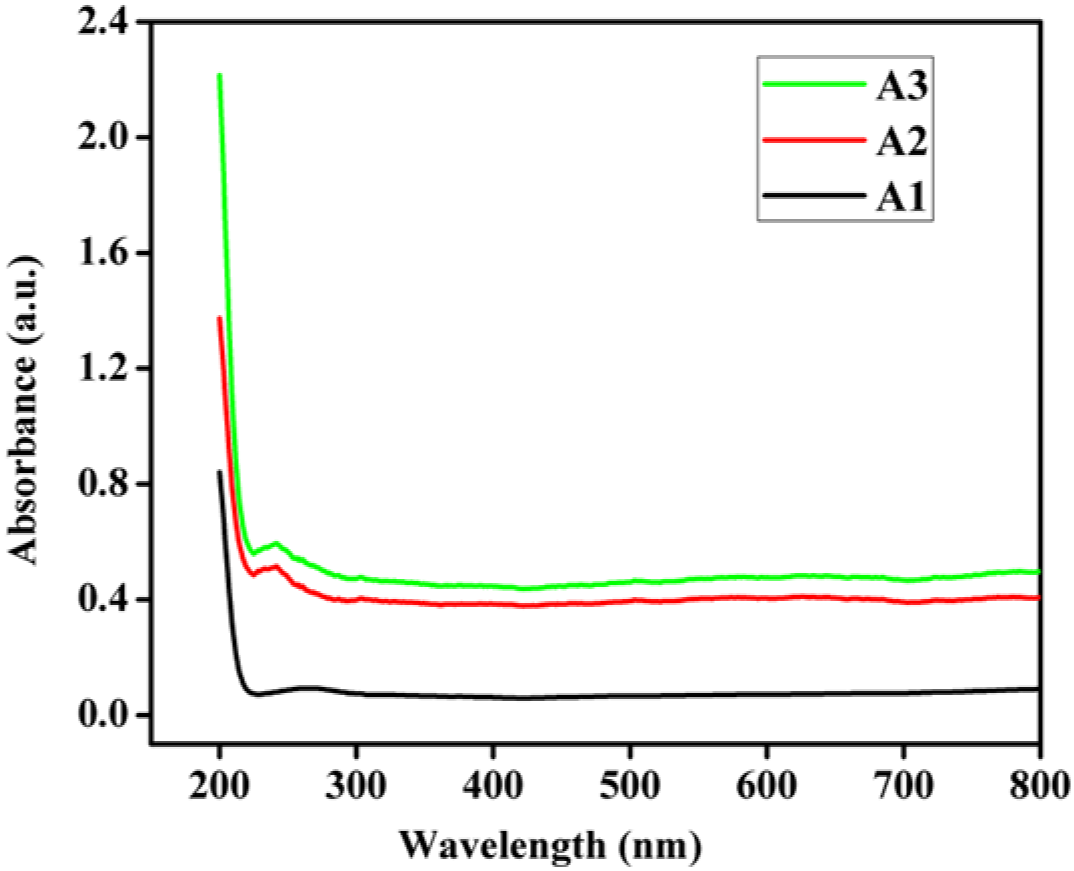

Figure 3

UV pattern of NiO/CuO nanocomposite different compositions

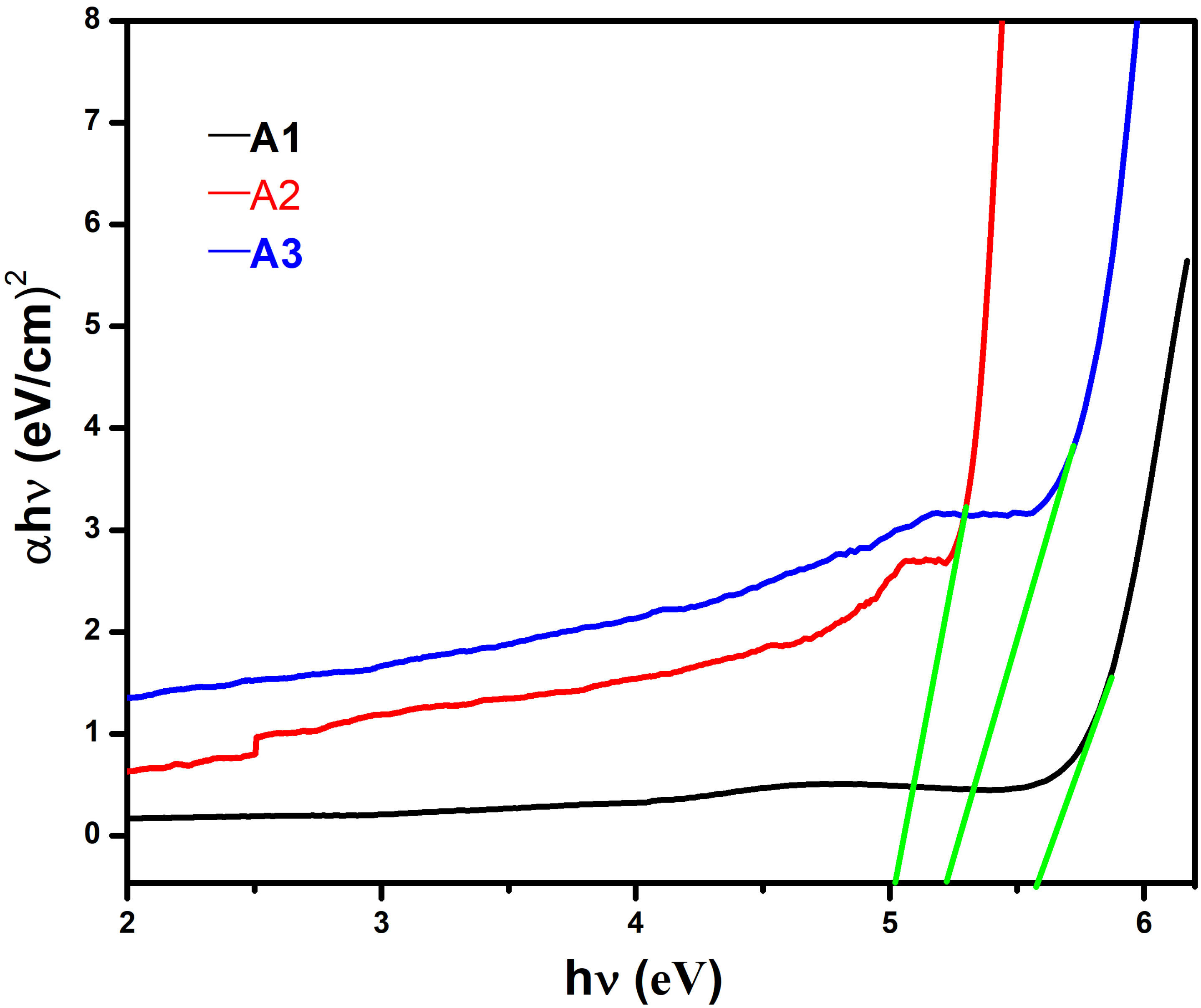

Figure 4

UV bandgap energy for NiO/CuO nanoparticles combined with VN leaf using different compositions

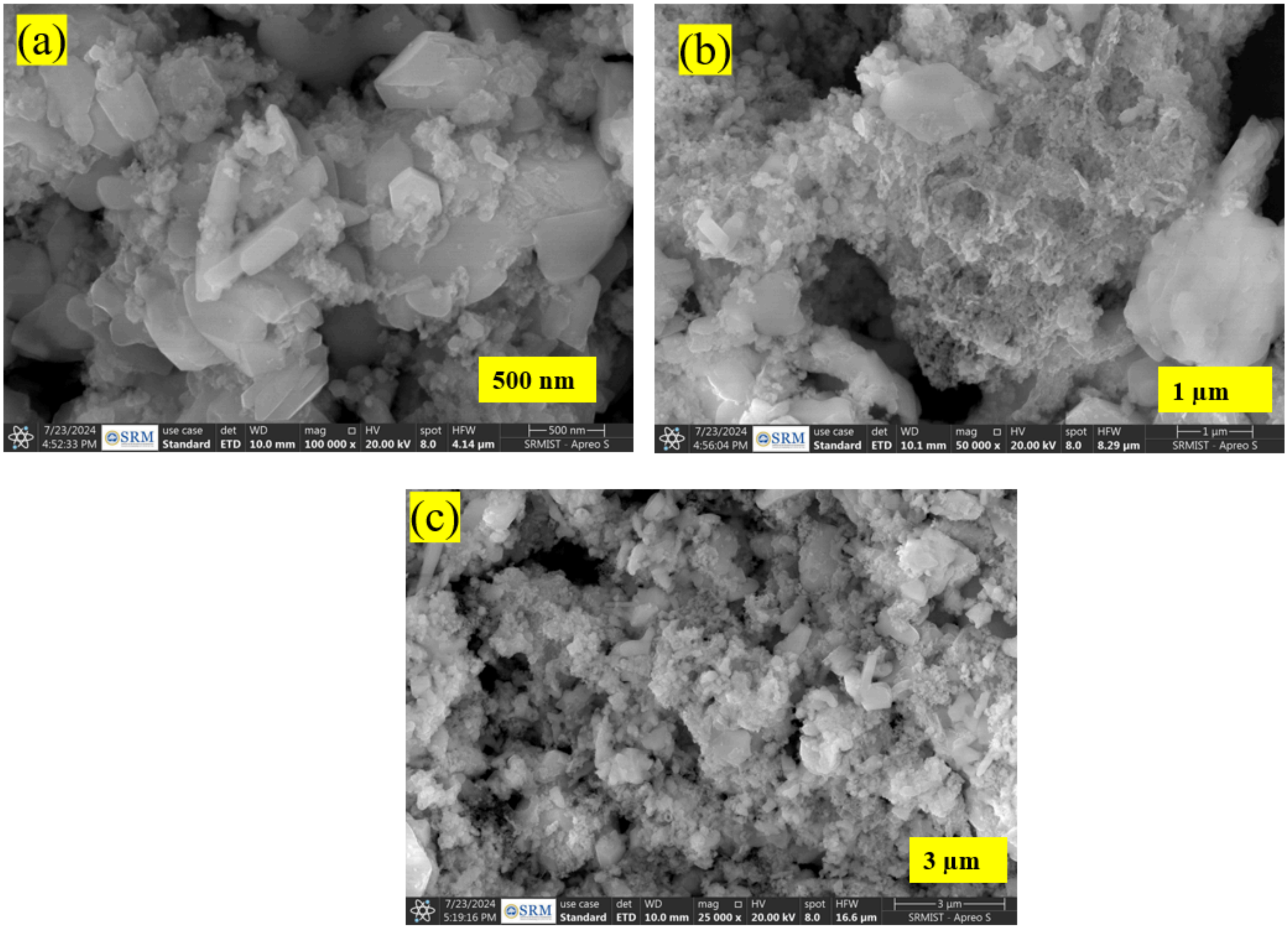

Figure 5

HR-SEM images of A1 composition NiO/CuO nanoparticles combined with VN leaf at different magnification

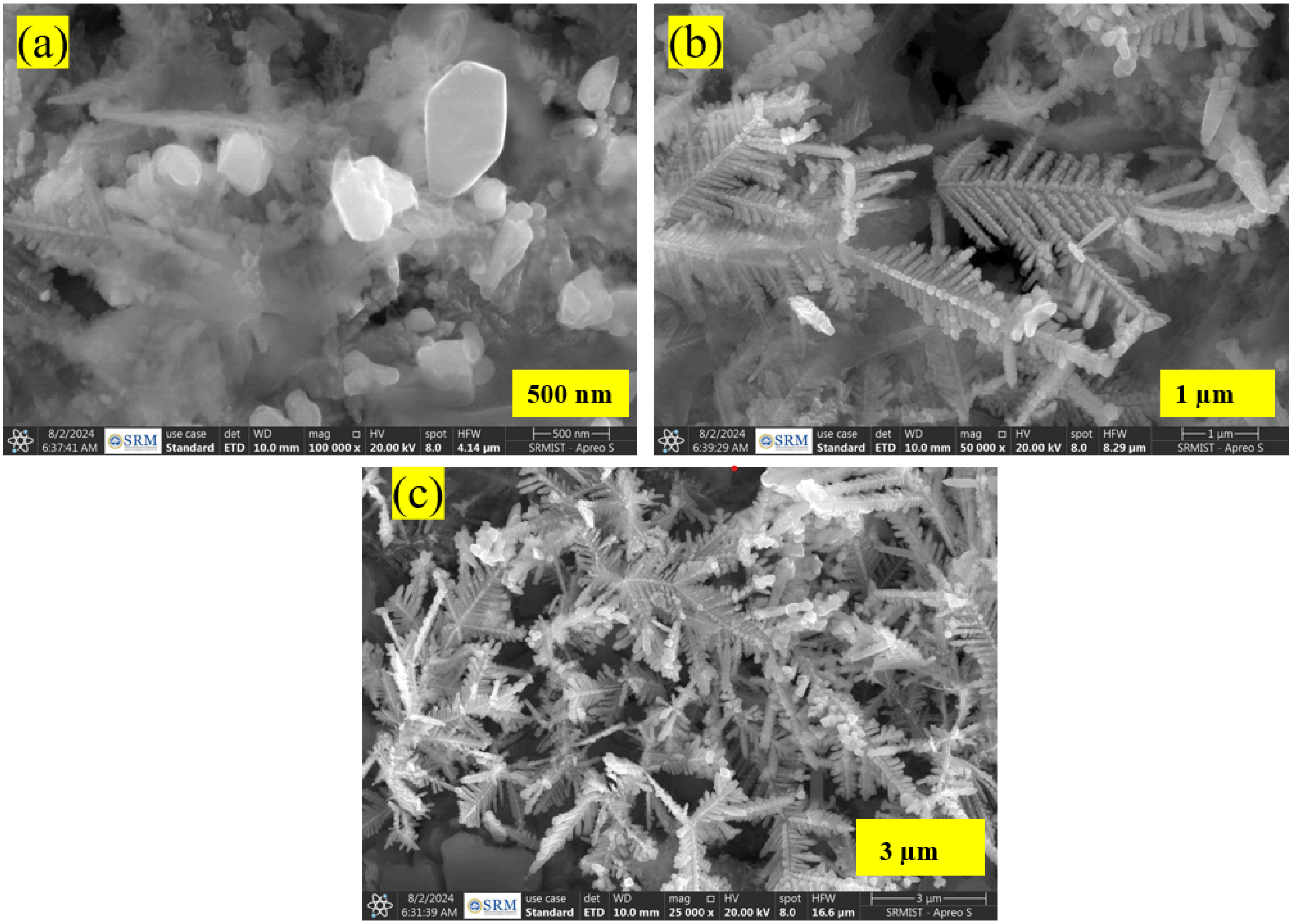

Figure 6

HR-SEM images of A2 composition NiO/CuO nanoparticles combined with VN leaf at different magnifications

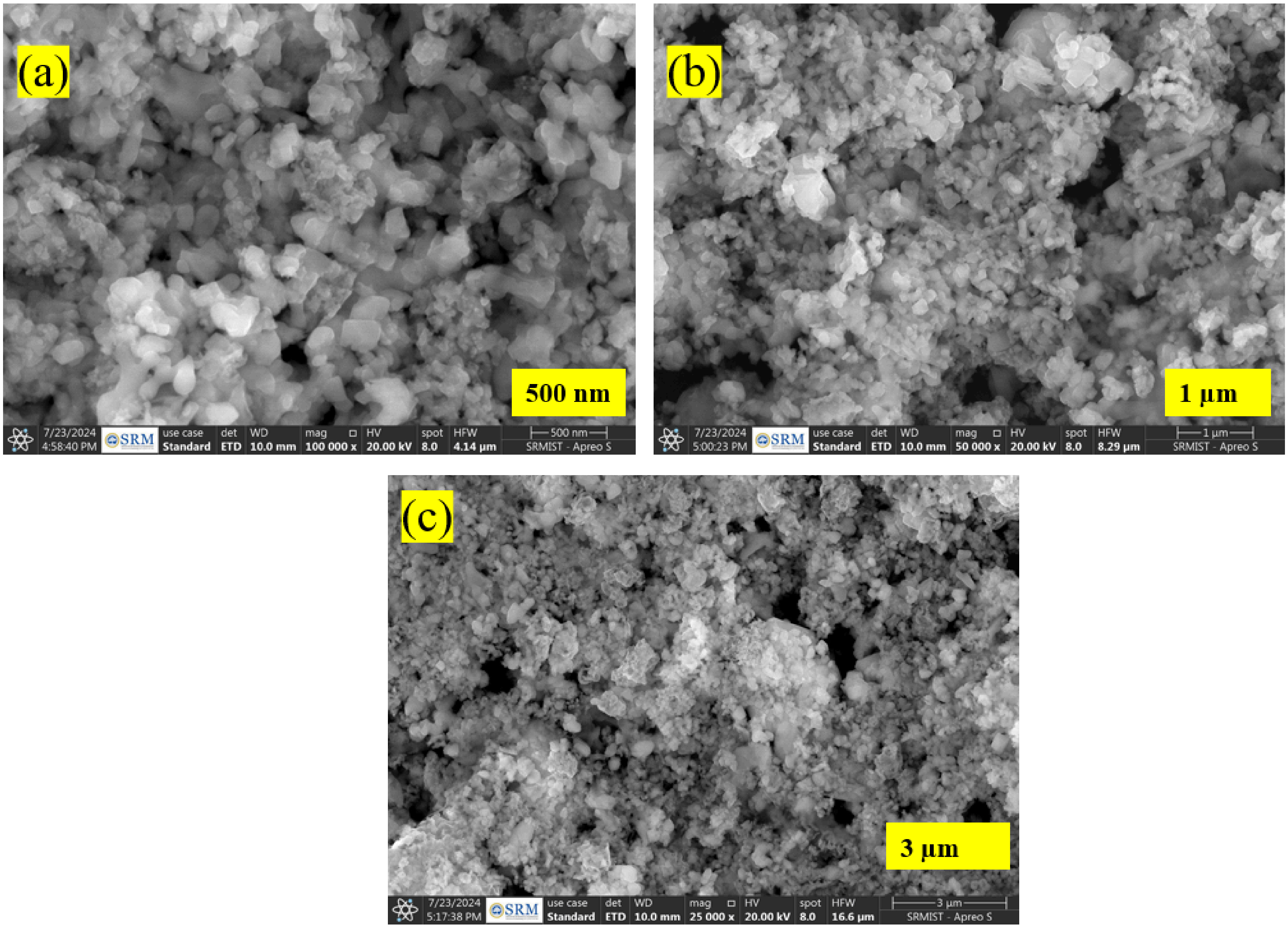

Figure 7

HR-SEM images of A3 composition NiO/CuO nanoparticles combined with VN leaf at different magnifications

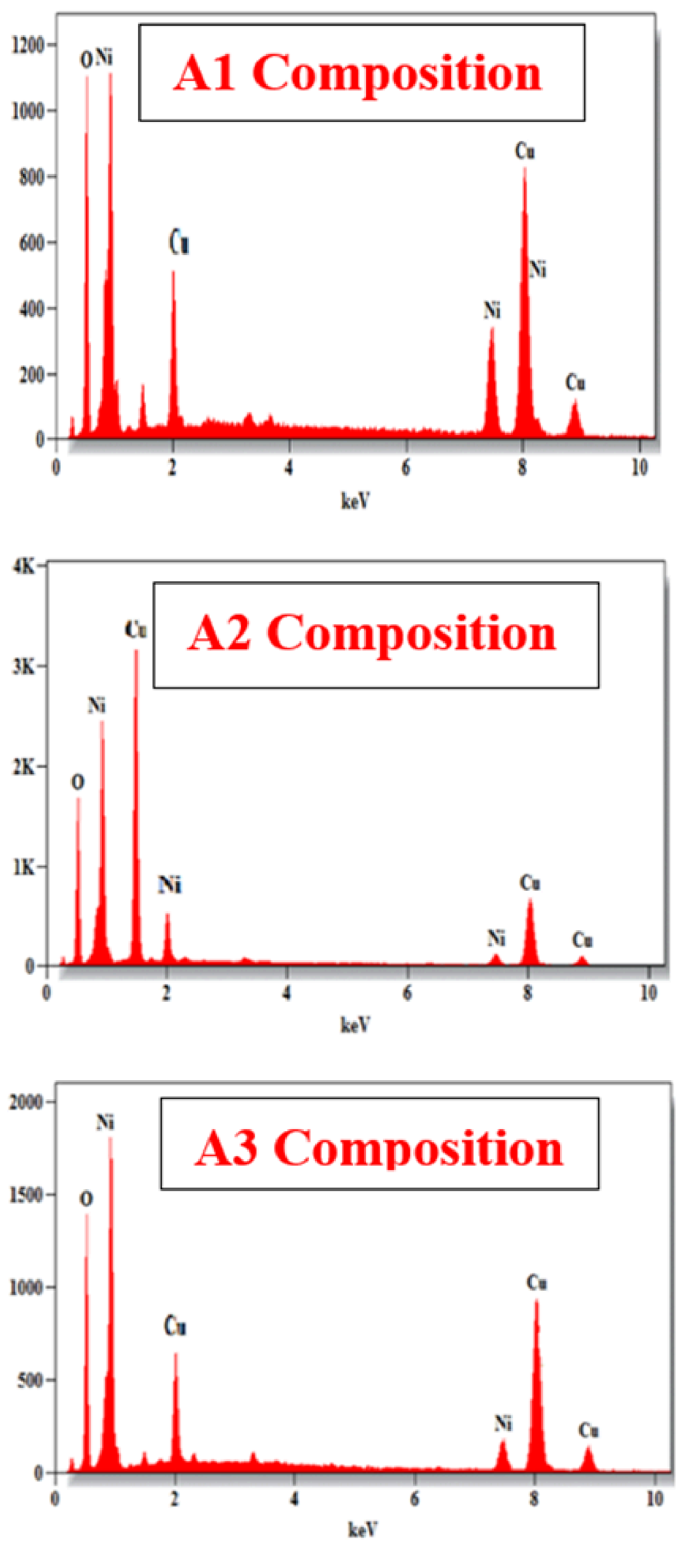

Figure 8

EDAX spectrum-3 different compositions

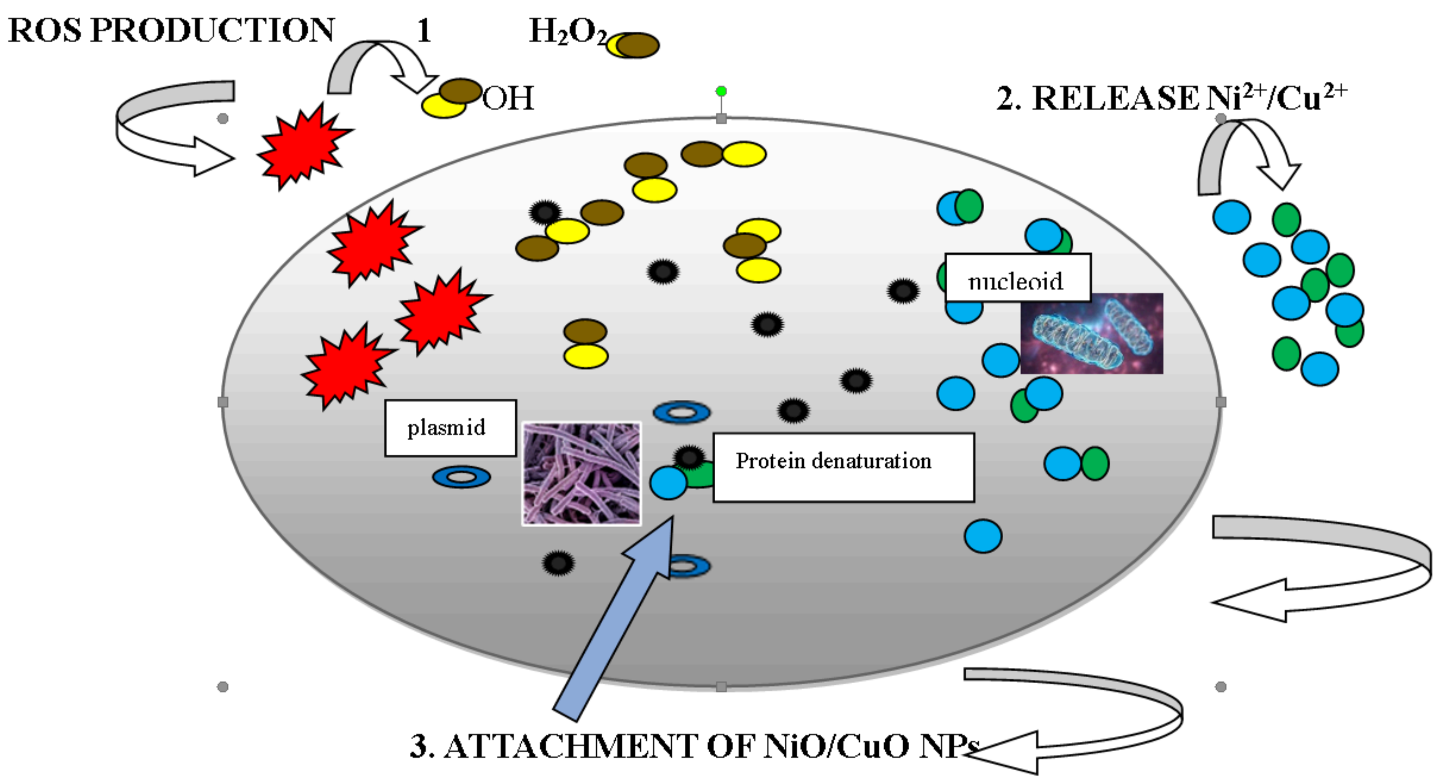

Figure 9

Antibacterial activity of NiO/CuO nanoparticles combined with VN leaf using different compositions A1, A2, and A3

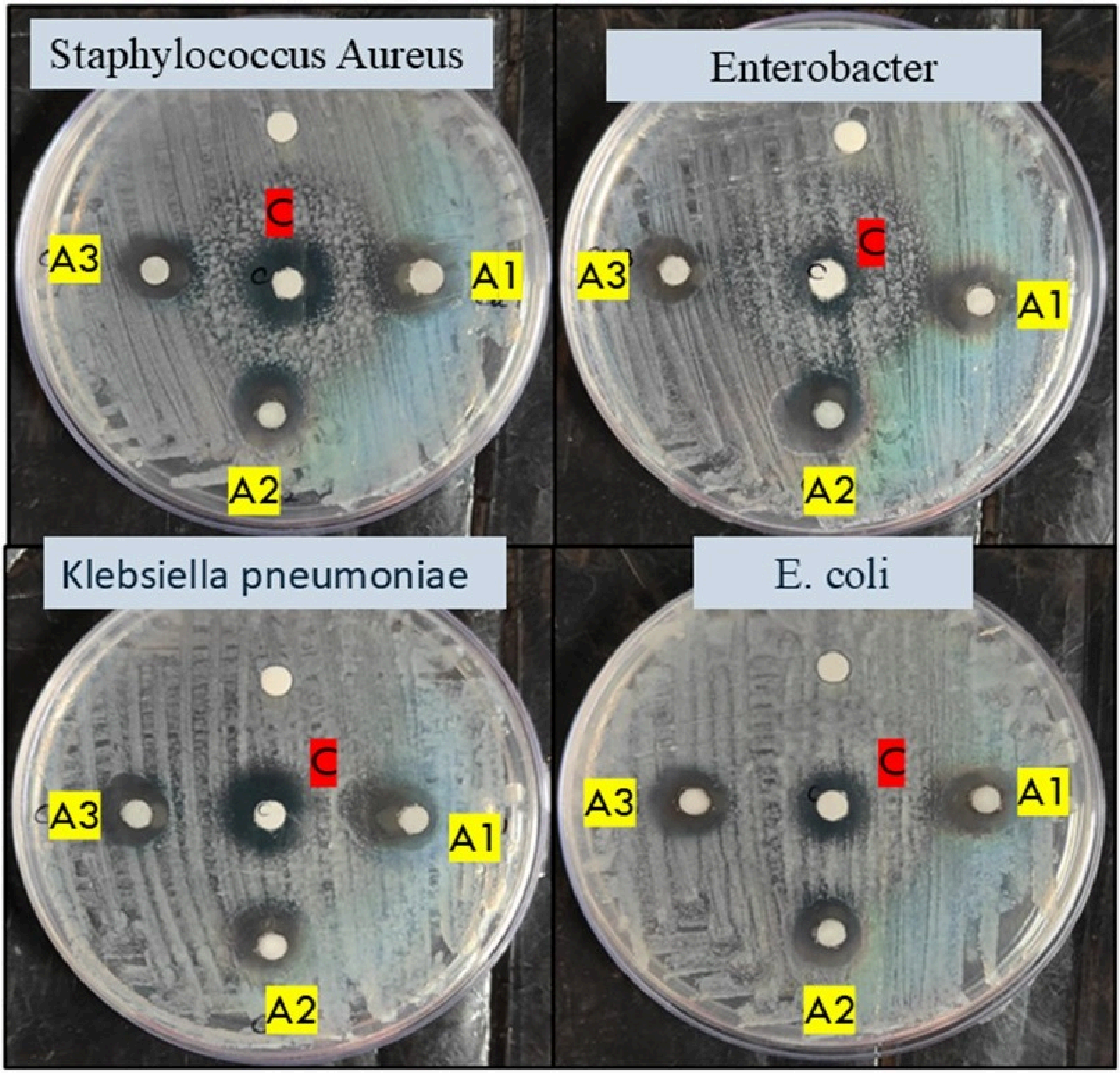

Figure 10

Antibacterial activity of NiO/CuO nanoparticles combined with VN leaf using different compositions A1, A2, and A3

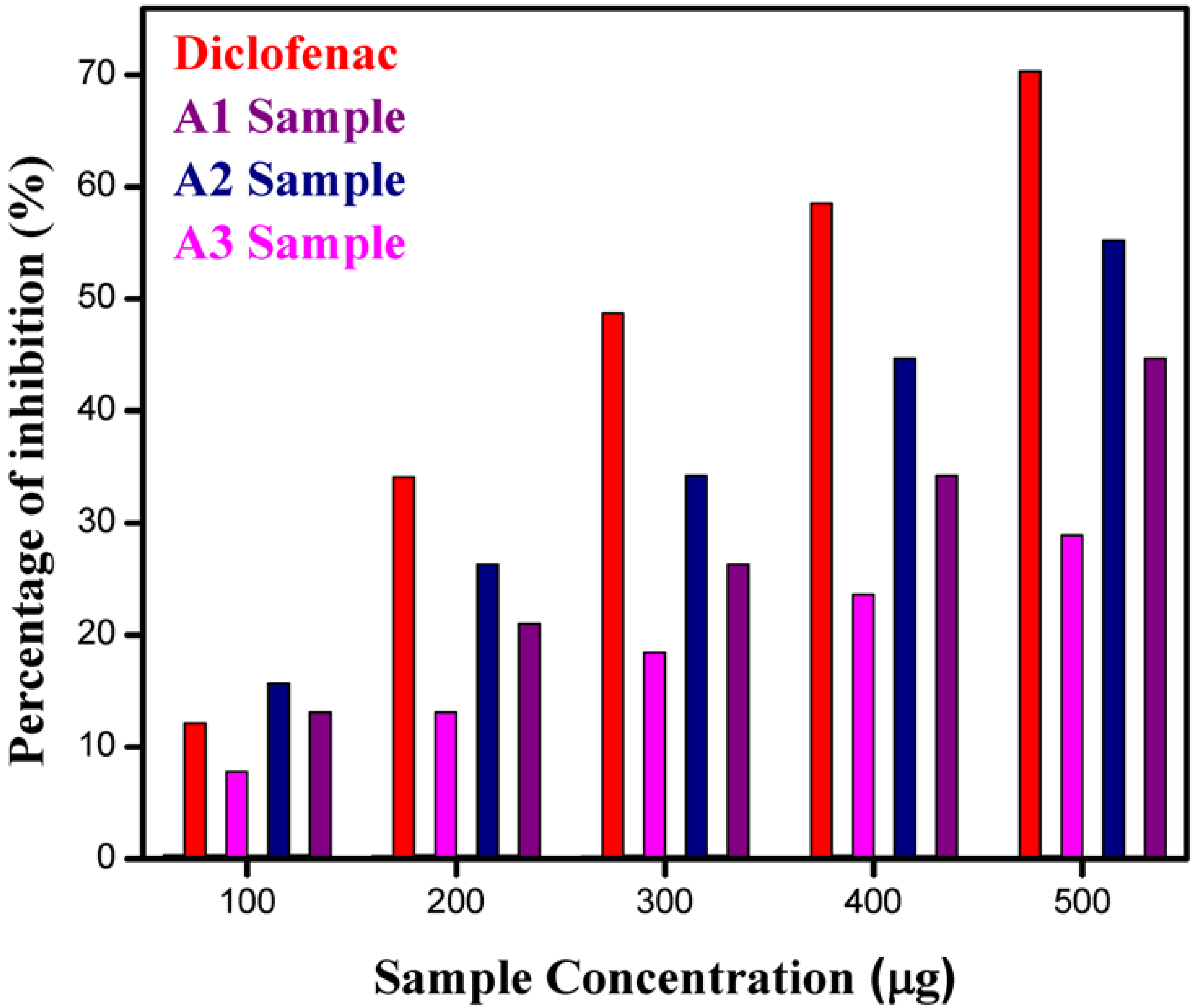

Figure 11

Anti-inflammatory activity of NiO/CuO nanoparticles combined with VN leaf using different compositions A1, A2, and A3

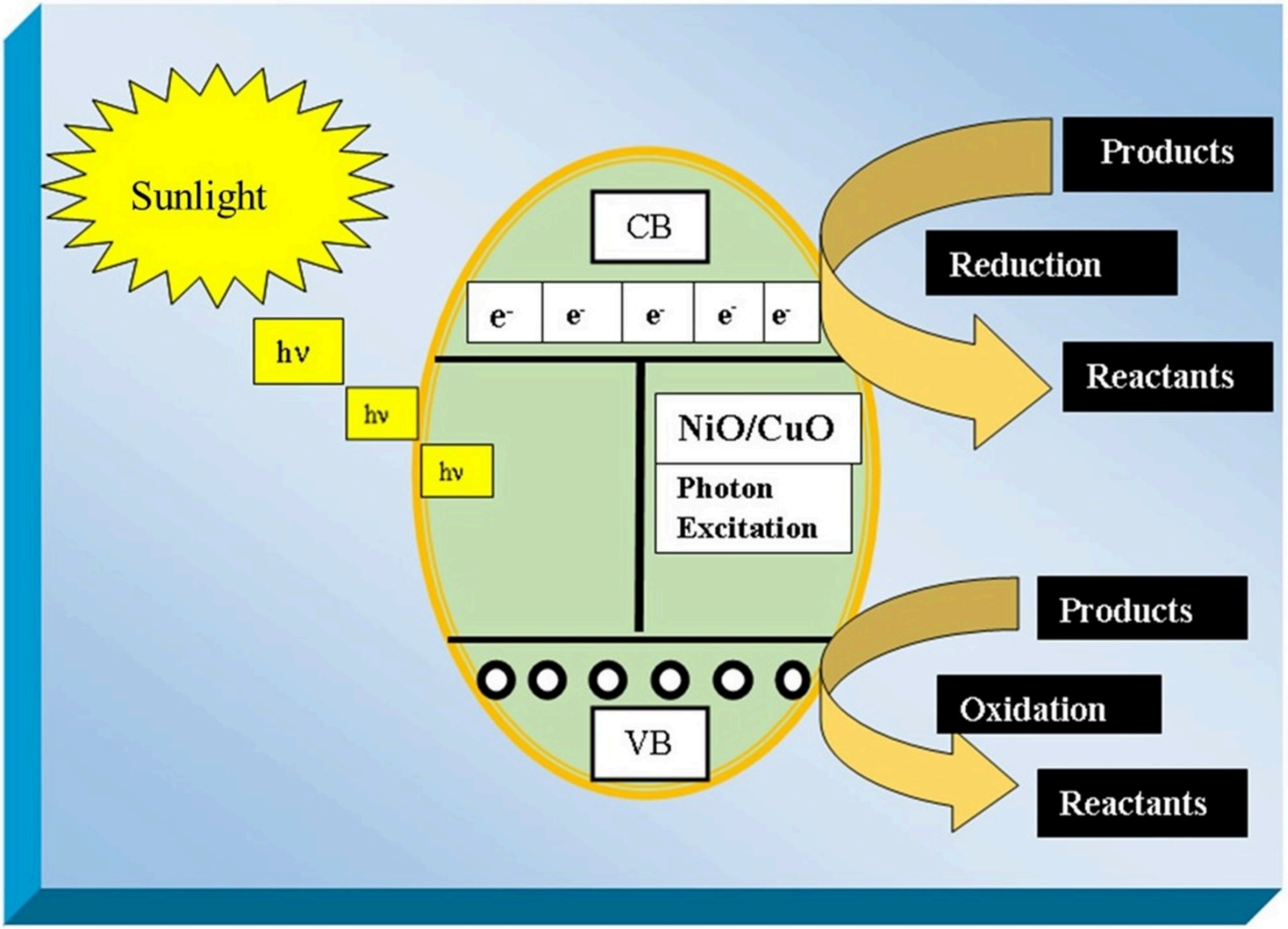

Figure 12

Mechanism of Photocatalytic activity of NiO/CuO nanoparticles combined with VN leaf using different compositions A1, A2, and A3

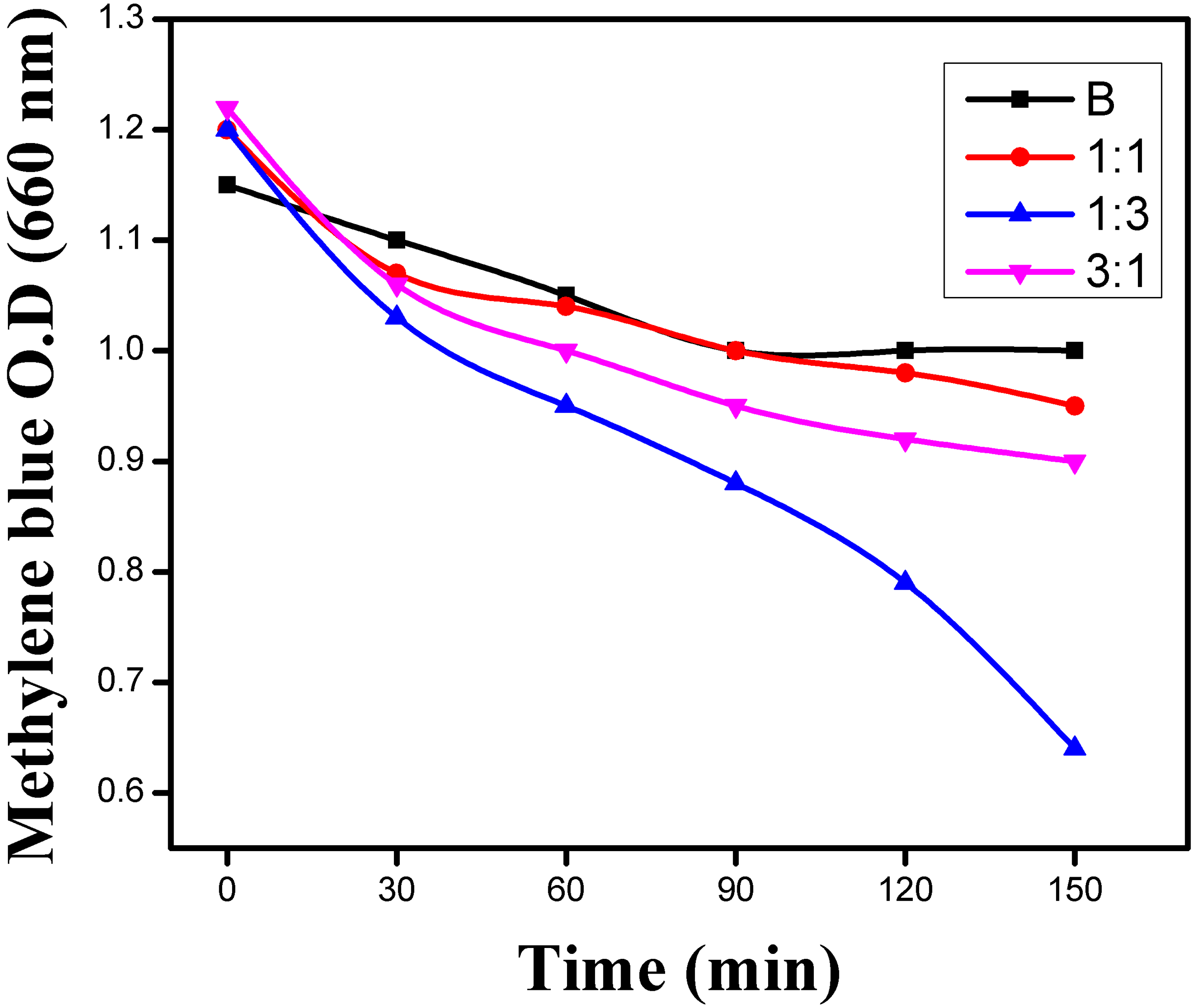

Figure 13

Photocatalytic activity of NiO/CuO nanoparticles combined with VN leaf using different compositions A1, A2, and A3